JOURNAL OF AGRICULTURAL AND FOOD CHEMISTRY

Anhydrous Goat's Milk Fat: Thermal and Structural Behaviors Studied by Coupled Differential Scanning Calorimetry and X-ray Diffraction. 2. Influence of Cooling Rate

WAFA BEN AMARA-DALI,[†,‡] PIERRE LESIEUR,[§,||] FRANCK ARTZNER,[⊥] NADIA KARRAY,[‡] HAMADI ATTIA,[‡] AND MICHEL OLLIVON*[,†]

Equipe Physico-Chimie des Systèmes Polyphasés, UMR 8612 du CNRS, Université Paris-sud, 5 rue J.B. Clément, 92296, Châtenay-Malabry, France, Unité d'Analyses Alimentaires, ENIS, BPW 3038 Sfax, Tunisia, Laboratoire pour l'Utilisation du Rayonnement Electromagnétique, Bâtiment 209D, Université Paris-sud, 91898 Orsay, France, Physico-Chimie des colloïdes, Université Henri Poincaré, UMR 7567 BP 239, 54506 Vandœuvre-lès-Nancy, France, and Laboratoire de Physique de la Matière Condensée, UMR 6626, Université de Rennes 1, Rennes, France

Crystallization and melting properties of triacylglycerols (TGs) in anhydrous goat's milk fat (AGMF) are investigated by X-ray diffraction as a function of temperature (XRDT) coupled with high-sensitivity differential scanning calorimetry (DSC), using synchrotron radiation and Microcalix. The polymorphic behavior of AGMF was monitored by varying the cooling rates between 5 and 1 °C/min from 45 to −20 °C with their subsequent melting at 1 °C/min. Quenching of AGMF at −20 °C was also examined to determine the metastable polymorphic form of AGMF. At intermediate cooling rates, TGs in AGMF crystallize, from about 18 °C in two different lamellar structures with triple chain length 3Lα stacking of 72 Å and a double chain length 2Lα stacking of 48 Å, which are correlated to two overlapped exothermic peaks recorded by DSC. A reversible transition sub α ↔ α was observed. Subsequent heating at 1 °C/min shows numerous structural rearrangements before final melting. At fast cooling of AGMF (5 °C/min), similar unstable crystalline varieties are formed while three endotherms are recorded. Several new unstable lamellar structures are observed after quenching. All of these data are compared to those previously reported at slow cooling (0.1 °C/min) showing a relative stability of the structures formed. In spite of general similitude, the thermal and structural behavior of the goat's milk is more complex than that of the cow's milk.

KEYWORDS: Goat's milk fat; polymorphism; triacylglycerols; X-ray diffraction; differential scanning calorimetry; crystallization

INTRODUCTION

Goat (*Capra hircus*) milk production is of significant importance to the economy and survival of large populations of many countries in the world, in developing countries as well as in developed countries (*1*). In the past decade, there has been an increased interest for goat milk production and its conversion to value-added products like cheese, UHT milk, and goat's milk powder. Besides water, the main component of goat milk is fat. Goat's milk fat (GMF) plays an important role in dairy products, especially by contributing the typical and unique flavors, tastes, and aromas (*2*, *3*). The composition of GMF is of tremendous importance for its market and nutritive values, through its technological and sensory properties of many goat dairy products (*4*). Among fats, milk fat exhibits the most complex lipid composition. Bovine milk fat is mainly composed of triacylglycerols (TGs) that represent about 98% of the total lipid. The other components included are diacylglycerols, monoacylglycerols, free fatty acids (FAs), phospholipids, sterols, and other polar lipids (*5*, *6*). Their respective concentrations depend on possible lipolysis. More than 400 FAs and 200 TGs have been identified (*7*). The complexity of its composition is in relation to its physical behavior. This chemical composition plays a critical role in dairy products because of its influence on aspects of technology (melting point, crystallization, etc.), physiology (biosynthesis), and nutrition (action of lipolytic enzymes). Milk fats including anhydrous goat's milk fat (AGMF) and anhydrous bovine's milk fat (ABMF) have complex FA and TGs compositions and display broad melting ranges and no true melting points. The thermal behavior of fats is usually studied by differential scanning calorimetry (DSC). However, the complex DSC recordings are difficult to interpret.

* To whom correspondence should be addressed. Tel: 33(1)46-83-56-29. Fax: 33(1)46-83-53-12. E-mail: michel.ollivon@u-psud.fr.
[†] Equipe Physico-Chimie des Systèmes Polyphasés.
[‡] Unité d'Analyses Alimentaires.
[§] Université Paris-sud.
[||] Université Henri Poincaré.
[⊥] Université de Rennes 1.

10.1021/jf063210p CCC: $37.00
Published on Web 05/12/2007

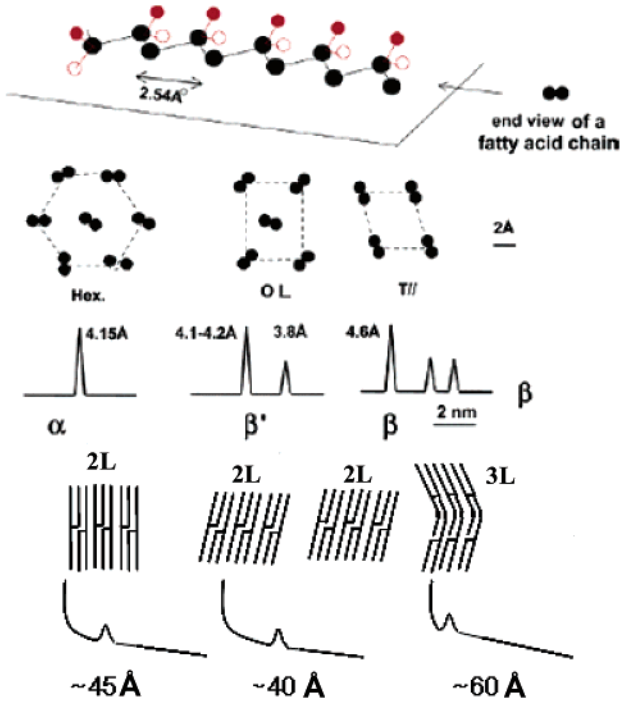

Figure 1. Main types of TGs packings. The main structural arrangements of TGs are shown. (Top) The stable conformation of the hydrocarbon chains of saturated FA is a planar zigzag shown here as a 3D view along its main axis (note that most of the front hydrogens are not drawn for clarity); on the right is the end view of the carbon zigzag. (Middle) Three main types of chain lateral packings (only carbons atoms are drawn as the end view above; hydrogen atoms are not drawn) corresponding to hexagonal (Hex.), orthorhombic perpendicular (O⊥), and triclinic parallel (T//) subcells and corresponding to α, β', and β forms, respectively. The corresponding longitudinal packings are shown at the bottom. X-ray characteristic lines are given for both lateral and longitudinal packings.

The composition of the crystals, which depends on crystallization conditions through the monotropic character of TGs polymorphism, changes during melting and sometimes even during crystallization (*8*, *9*). Thus, identification of the species, the domain of existence of which is delimited by each melting or crystallization DSC peak, is often impossible without the help of techniques that yield information about structures (X-ray or neutron diffraction, infrared spectroscopy, etc.) (*10*, *11*). X-ray diffraction (XRD) has been recognized as an essential tool for elucidating the polymorphism of fats since it complements DSC. Lipid polymorphism results from the different possibilities of lateral packing of the FA chains and of longitudinal stacking of molecules in lamellae (*12*). The longitudinal and lateral packing are recorded by XRD at small and wide angles, respectively, as detailed in **Figure 1** (*13*).

Access to X-ray high-flux sources (synchrotron) permits the study of the polymorphism and the transitions displayed by complex TGs mixtures as a function of temperature and the comparison of these data to DSC recordings (*14*). Thanks to the coupling of DSC and XRD as a function of temperature (XRDT), the thermal and structural behaviors of ABMF at different cooling rates (from 0.1 to 1000 °C/min) were studied by Lopez et al. (*15*−*18*). Using these techniques, the thermal and structural behaviors of anhydrous camel milk fat have also been recently studied by Karray et al. (*19*, *20*). The authors examined the crystalline structures formed by TGs during slow (0.1 °C/min), intermediate (1 °C/min), and fast (5 °C/min) cooling of these milk fats and their evolutions as a function of temperature during subsequent heating at 1 or 2 °C/min.

The aim of this series of papers is to examine the crystalline structures formed by TGs of AGMF and their polymorphism. In this second and last paper of the series, AGMF is submitted to fast and intermediate cooling rates as well as to quenching. To determine the stability of the crystalline varieties formed during cooling, their evolutions were also followed during a subsequent heating at 1 °C/min. We compare our results with those obtained during slow cooling at 0.1 °C/min (*21*).

MATERIALS AND METHODS

Samples. Goat milk was obtained from a goat herd (Alpine race) belonging to the Arid Region Institute (ARI, Medenine, Tunisia). Sodium azide, NaN_3, was added to milk at a concentration of 0.02% (w/v) to prevent the growth of bacteria. Cream was obtained from the refrigerated mixed goat milks after centrifugation three times at 25 °C and 3000*g* for 20 min on a Jouan GR 20 22 centrifuge (Jouan, Saint Herblain, France). The procedure of extraction of AGMF from cream is similar to that used previously (*21*). Briefly, after manual churning of cream (at $T = 12-15$ °C), 10 g of butter was melted to 60 °C and centrifuged for 2 min at 3000*g*. The upper organic phase AGMF was separated and filtered at 50 °C in the presence of sulfate anhydrous sodium (Na_2SO_4) on a filter of glass wool.

DSC Measurements. Thermal analysis of AGMF was conducted with a DSC-7 Perkin-Elmer (St. Quentin en Yvelines, France) equipped with a cooling device (Intracooler II) in dry air atmosphere and running under Pyris Thermal Analyzing systems Software (version 3.52). AGMF samples were loaded in aluminum pans of 40 μL as previously described (*21*). AGMF samples were heated at 70 °C during 5 min in order to melt all crystals and nuclei. Crystallization curves were recorded from 60 to −40 °C at different cooling rates: 0.1, 0.3, 1, 3, and 5 °C/min. Then, following cooling, all of the melting curves were recorded from −40 to 60 °C at 1 °C/min.

XRDT/DSC Measurements. Experiments were performed using a technique that allows simultaneous synchrotron radiation XRD as a function of temperature (XRDT) and high-sensitivity DSC, Microcalix, which was carried out in the same apparatus (*22*, *23*). The experiments were conducted on D_{22} bench of the synchrotron beam at LURE (Laboratoire pour l'Utilization du Rayonnement Electromagnétique, Orsay, France), using the setup described previously (*21*). Briefly, two linear detectors allowed the recording of simultaneous small- ($q = 0-0.45$ Å^{-1}) and wide- ($q = 1.1-2.1$ Å^{-1}) angle XRD patterns with sample to detector distances of 177 and 30 cm, respectively. Both XRDT data and DSC signals were simultaneously collected from the same sample (about 25 mg) with a single computer in order to avoid any time or temperature shift in the data collection. Standardization of X-ray detection and DSC analysis was already described (*21*). The channels of the detectors were calibrated to express the XRDT data in the scattering vector q with $q = 4\pi \sin(\theta)/\lambda = 2\pi/d$, where q is in Å^{-1}, θ is the angle of incidence of X-ray relative to the crystalline plane, λ is the X-ray wavelength, and d in Å is the repetition distance between two planes. The crystallization behavior of AGMF was conducted on cooling at 5 and 1 °C/min from 45 to −20 °C at $dT/dt = 1$ and 5 °C/min using capillary-contained samples. The melting behavior was monitored by heating of the samples at $dT/dt = 1$ °C/min. Quenching of AGMF at −20 °C was also examined. Each XRD pattern recorded as a function of temperature simultaneously at small and wide angles was analyzed using IGOR PRO 4.0 software (Wavemetrics, United States) as previously described (*21*). On figures generated from IGOR analysis, the size of symbols was proportional to the maximum of intensity of the line while the circle center position indicated period. Moreover, the DSC crystallization curve, which was recorded simultaneously, was superimposed on top of the other results. As a consequence of the use of such representation, it was easier to link thermal events to structural changes.

Statistical Analysis. Statistical analysis was conducted as previously (*21*), but the XRDT patterns, which are synchrotron beam consuming, were only obtained once. However, because each frame was independent of the neighbor one, their evolution was considered more or less as a repetition of analysis.

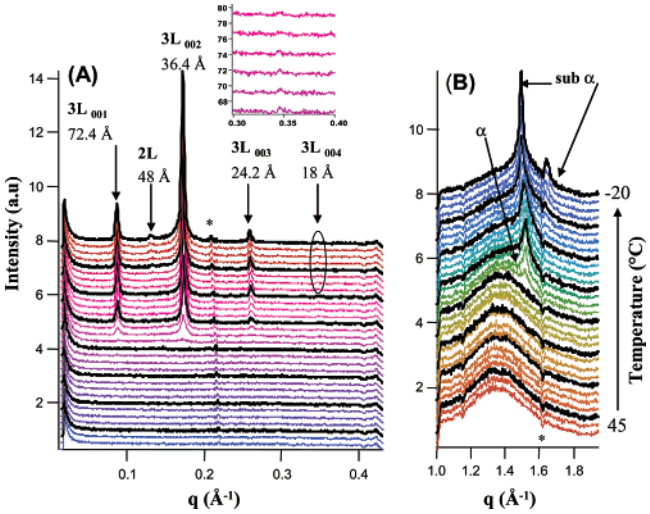

Figure 2. Three-dimensional plots of SAXD (**A**) and WAXD (**B**) patterns of anhydrous goat milk recorded from 45 to −20 °C, at intermediate cooling rate (1 °C/min) as a function of time, using coupled XRDT-DSC. (Asterisk symbols correspond to negative peaks due to wide-angle detector defects.) The crystalline structures identified are noted in the figure. The insert shows an enlargement of the domain delimited by an ellipse.

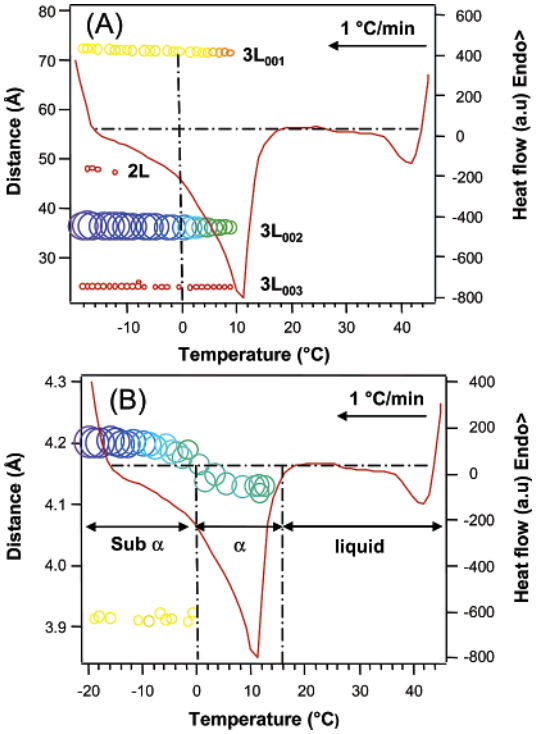

Figure 3. Evolutions, as a function of temperature of the LS (**A**) and SS (**B**), deduced from the diffraction peaks of **Figure 2** by IGOR analysis as in ref *21*. Both evolutions are superimposed with the DSC (raw data) crystallization curve recorded simultaneously during cooling of AGMF at 1 °C/min. Symbol sizes, centered on distance and temperature, are proportional to the maxima intensities of the lines.

RESULTS AND DISCUSSION

The structural and thermal properties of AGMF were studied at intermediate and fast cooling rates, respectively, at 1 and 5 °C/min, from 45 to −20 °C, by coupled XRDT and high-sensitivity DSC techniques. After such crystallization, the AGMF samples were subsequently analyzed on heating at 1 °C/min from −20 to 45 °C. On the other hand, we studied the formation of the most unstable crystalline structures formed by a sample of liquid AGMF, after its rapid quenching from 45 to −20 °C, as well as their evolutions as a function of time at −20 °C, and then on heating. Finally, the influence of the cooling rate on the thermal and structural behaviors is discussed by comparing the results of this study with that of the preceding paper of the series obtained at slow cooling rates (*21*).

1. Crystallization Behavior of AGMF at Intermediate Cooling Rate: 1 °C/min. *1.1. Cooling at 1 °C/min.* 1.1.1. Identification of the Crystalline Structures. The XRD patterns, recorded as a function of time at both small and wide angles during cooling of AGMF, are presented, vs temperature, as three-dimensional (3D) plots, in **Figure 2**. The small-angle X-ray diffraction patterns (SAXD) (**Figure 2A**) show the progressive development of four and then five diffraction lines corresponding to crystallization of TGs in goat milk fat, as a function of temperature. On cooling at 1 °C/min, at about $T =$ 10 °C, four sharp diffraction lines, centered at about $q = 0.09$, 0.17, 0.26, and 0.35 Å^{-1} (72.4, 36.4, 24.2, and 18 Å), are observed and detected by IGOR software, while the fifth one is observed but not detected. All of these diffraction lines increase simultaneously in intensity as a function of the decrease in temperature during cooling. This first crystalline form corresponds to a lamellar structure with a triple chain length organization (trilayered stacking, 3L). The line at 36.4 Å ($3L_{002}$) likely corresponds to the second order of that observed at 72.4 Å ($3L_{001}$) of the TGs molecules and the lines at 24.2 and 18 Å ($3L_{003}$ and $3L_{004}$) correspond to the third and the fourth orders, respectively (**Figure 2A**). From about $T = -10$ °C, a weak diffraction line corresponds to a second organization of the longitudinal packing of the alkyl chain of TGs in milk fat recorded at $q = 0.13$ Å^{-1} (48 Å). This crystalline form likely corresponds to a lamellar structure with a double chain length organization (bilayered stacking, 2L).

At wide angles, the recording of XRD allows identification of the lateral packing of the alkyl chains of acylglycerols in characteristic subcells. The wide-angle X-ray diffraction (WAXD) patterns simultaneously recorded as a function of temperature (**Figure 2B**) shows, at about 18 °C, the occurrence of a first diffraction line at $q = 1.51$ Å^{-1} (4.15 Å), which is characteristic of TGs crystallization with an hexagonal packing of the acylglycerols chains, called the α form. It is the most unstable packing of the acylglycerols chains. From about 0 °C, the occurrence of two diffraction lines centered at $q = 1.49$ (4.2 Å) and 1.7 Å^{-1} (3.7 Å) indicates the formation of a new crystalline arrangement of TGs in AGM corresponding to an orthorhombic packing of the chains also called the sub α form.

1.1.2. Spacing Evolution. The evolution of the long spacings (LS) and short spacings (SS), determined from the diffraction peaks recorded at small and wide angles in **Figure 2A**,**B**, vs temperature, is presented, respectively, in **Figure 3A**,**B**. **Figure 3** shows the plot of the spacing and intensity (circle diameter) of the line detected by software together with the corresponding DSC recording.

At small angles, the LSs of the diffraction lines related to the $3L_{001}$ (72.4 Å) variety and its corresponding superior orders $3L_{003}$ (24.2 Å) and $3L_{002}$ (36.4 Å), appearing at about 10 °C (**Figures 2A** and **3A**), do not show any significant evolution during cooling of the AGMF, meaning that no changes occur in the longitudinal stacking of TGs. On the other hand, for the line 2L (48 Å), observed below −10 °C, the thickness of this lamellar structure slightly increases as a function of temperature during cooling of AGMF. On the contrary, in the domain $0 < T < 12$ °C, the SS corresponding to an α form shows a slight increase from about 4.12 to 4.16 Å of the hexagonal subcell

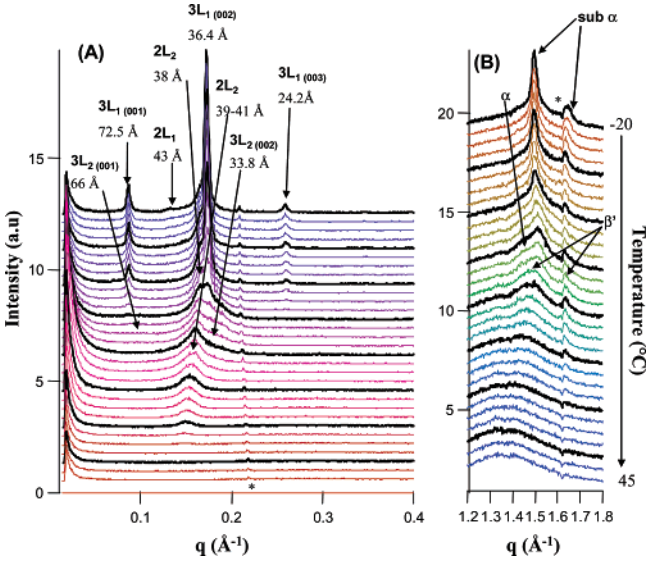

Figure 4. Three-dimensional plots of SAXD (**A**) and WAXD (**B**) patterns recorded as a function of time during heating of AGMF at 1 °C/min after cooling at 1 °C/min (asterisk as above **Figure 2**). The crystalline structures identified are noted in the figure.

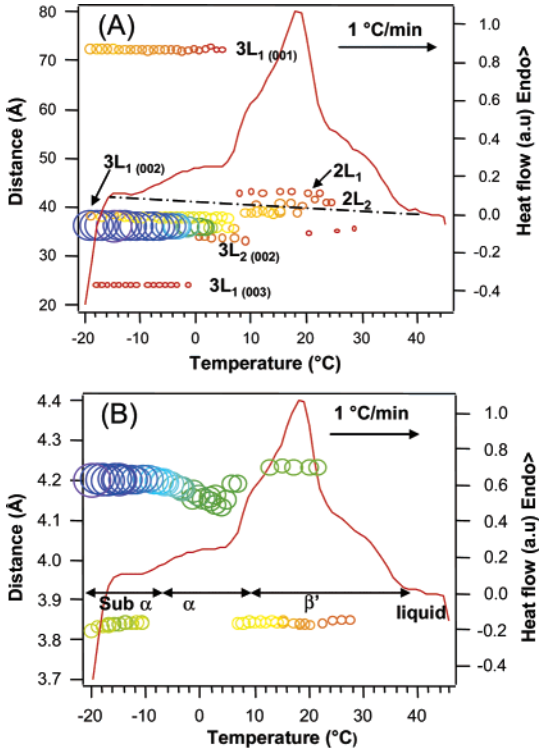

Figure 5. Evolutions, as a function of temperature of the LS (**A**) and SS (**B**) deduced from the diffractions peaks of **Figure 4** as above, are superimposed with the DSC crystallization curve recorded simultaneously during heating of AGMF at 1 °C/min, following its crystallization cooling at 1 °C/min. Symbol sizes, centered on distance and temperature, are proportional to the maxima intensities of the diffraction peaks.

(**Figures 2B** and **3B**). This evolution indicates that this packing becomes less dense upon increasing up to 4.16 Å. From about 0 to −20 °C, this line splits into two lines at SS = 3.93 and 4.2 Å. This split is related to the occurrence of an orthorhombic packing sub α. The α ↔ sub α reversible polymorphic transition observed for SS might correspond to the blocking in a tight packing of the FA chains (see below).

1.1.3. Intensity Evolution. The evolutions of maximum intensity of diffraction peaks recorded at intermediate cooling rate of AGMF were plotted on the same graph (**Figure 3A**,**B**) as a function of temperature, in order to relate the longitudinal organization of the TGs molecules to their lateral packing (the symbol sizes are proportional to the maximum line intensities). At small angles, the intensity of the line $3L_{002}$ (36.4 Å) increased from its formation at about 10 to 0 °C. This increase, which is correlated with an intensity increase of α at SS, should correspond to a relatively fast crystallization (**Figure 3**). At $T < 0$ °C, the diffraction lines $3L_{001}$, $3L_{002}$, and $3L_{003}$ are stable in intensity. At wide angles, the intensity of the α form is stable from 10 to −10 °C whereas it increases at $T < -10$ °C. Surprisingly, this intensity increase is not correlated with the split of the main WAXD line characterized by a shift of the main line and the occurrence of a second line at 3.93 Å. The same transition has already been observed in bovine cream crystallization (*24*). The α organization corresponds to a random hexagonal packing of the chains in which an average one kink per chain is observed. As the temperature is lowered, progressively, the chains rotate less rapidly and pack together more tightly in the sub α form.

When $T > 18$ °C, SAXD and WAXD patterns show that milk fat TGs are in their liquid state. We concluded that the following transitions are observed on cooling:

$$\text{liquid} \rightarrow \alpha \leftrightarrow \text{sub } \alpha$$

as shown in **Figure 3**.

1.1.4. Thermal Properties. The DSC crystallization curve was recorded simultaneously with XRD from the same sample of AGMF during its cooling at 1 °C/min, thanks to XRDT/DSC coupling (**Figure 3**). First of all, the signal recorded by the DSC between 45 and 37 °C should not be taken into consideration since it corresponds to the equilibration of the calorimeter. The DSC recording shows two or three (see below) overlapped exothermic events, which can be related with the formation of the lamellar structures analyzed above. The initial crystallization temperature is about 18 °C. The first exothermal event recorded on cooling from about 18 °C corresponds to crystallization of TGs incorporated in the trilayered α structure characterized by a period of 72.4 Å and four LS lines ($1 < l < 4$). The second exothermal event recorded from about 0 to −18 °C corresponds to the formation of a 2L structure, likely sub α.

1.2. Heating of AGMF at 1 °C/min. Following crystallization upon cooling at 1 °C/min, the AGMF sample was immediately heated from −20 to 45 °C at 1 °C/min in order to monitor the polymorphic evolution of the crystalline structures formed during cooling.

1.2.1. Structural Analysis. The plots of the XRD patterns recorded, as a function of time, at small and wide angles are presented in **Figure 4A**,**B**, respectively, vs temperature as 3D views. The evolutions of the small-angle lines show successive and complex phase transitions of the crystalline structures (**Figure 4A**). The evolutions of maximum intensity of diffraction peaks recorded at small and wide angles as a function of time during heating of AGMF were plotted on the same graph (**Figure 5A**,**B**) as a function of temperature. We can define at least four temperature-delimited domains. First, the line at 43 Å fast disappears on heating between −20 and −10 °C. Indeed, in the interval of temperature -20 °C $< T < -2$ °C, both intensity and position of the set of diffraction lines of the crystalline variety, 3L at 72.5 Å, are quasi-constant. At $T > -2$ °C, the decrease in intensity observed is interpreted as the melting of this triple chain length structure to the benefit of a more stable form. At $T > 8$ °C, this set of lines has disappeared

while a 2L variety appeared, the period of which is changing from about 38 to 41 Å as shown by the drift of line position (**Figure 5A**). The evolution of SAXD patterns of **Figure 4A** shows more clearly the formation, the drift, and the successive melting of this form than the plot of **Figure 5A** due to peak overlapping. However, the comparison of the line intensity of this $2L_2$ more stable form with that of the 3L metastable form observed seems to indicate that the crystallization is not complete. To further crystallize this variety, a conditioning at a temperature close to that of its formation would have been required. The comparison of the characteristics of the crystalline forms observed during heating after cooling at 1 °C/min, with that observed on slow cooling (0.1 °C/min), shows that the line at 39−41 Å formed during heating corresponds to that observed previously at a slower rate (*21*). Similarly, the brief occurrence of a line at 33.8 Å (and simultaneously corresponding to a possible bump at about 66 Å) was interpreted as the beginning of the formation of the $3L_2$ observed previously (*21*).

Concerning the chain packing, the X-ray lines of which are observed at wide angles (**Figure 1**), it was not possible to distinguish the lateral packing of minor forms. The main lines correspond to sub α, α, and β′. The reversibility of the transition observed around −5 °C between sub α and α, which are the less stable polymorphic forms, is clearly observed in **Figures 2B** and **4B** as a reversible transition between hexagonal (α, line at about 4.15 Å) and orthorhombic (sub α, lines at 3.7 and 4.2 Å) packings (**Figures 3B** and **5B**). This reversible transition attributed to the major lines $3L_1$ is surprisingly not accompanied by any detectable change of the longitudinal stacking (**Figures 2B** and **4B**). The fact that an orthorhombic chain packing transforms into a hexagonal one and consequently a more ordered packing transforms into a less stable one on heating is apparently a paradox. In fact, it is not surprising since the sub α ↔ α transition is not monotropic but enantiotropic. Contrary to what is observed for other TGs transitions, this solid−solid sub α ↔ α reversible transition does not imply chain melting (*25*) and it is not accompanied by any LS change. For $T >$ 6 °C, the lines observed at about 4.2 and 3.8 Å characteristic of the β′ crystal are correlated with the occurrence of the structure $2L_2$. These results show that α → β′ polymorphic transitions occur during heating. So, we are in the presence of three successive transitions at delimiting four different temperature domains. We did not record any diffraction lines at $T \geq$ 38 °C, meaning that all of the TGs of AGMF are in their liquid state.

As a summary, the following polymorphic transitions are observed on heating:

$$\text{sub } \alpha \leftrightarrow \alpha \rightarrow \beta' \rightarrow \text{liquid}$$

to which the following varieties correspond

$$\alpha\ 3L_1\ (72.5\ \text{Å}) \rightarrow \beta'\ 2L_1\ (38-41\ \text{Å}) \rightarrow \text{liquid}$$
$$+\ \beta'\ 3L_1\ (65-66\ \text{Å}) \rightarrow \text{liquid}$$
$$+\ \alpha?\ 2L_1\ (43\ \text{Å}) \rightarrow \text{liquid}$$

It is interesting to note that similar polymorphic transitions are observed in ABMF at heating at 2 °C/min after cooling at 3 °C/min but at different transition temperatures (*18*).

1.2.2. Thermal Analysis. Thanks to the above XRD analysis, the complex melting curve recorded by DSC during heating at 1 °C/min of the AGMF sample is interpreted as shown in **Figure 5**. The DSC melting curve shows the overlapping of 3−4 endotherms until the final melting temperature at about 38 °C. These endothermic peaks correspond to the low melting point, medium melting point, and high melting point. The temperature range of the first melting endotherm, which is located in the interval $-16\ °C < T < 6\ °C$, has been assigned to the melting of part of the α 3L form. The second endotherm, which is observed in the range $6\ °C < T < 22\ °C$, coincides with both the transition and the melting of both β′ $2L_1$ and α $3L_1$. The last endotherm corresponds to that of β′ $2L_1$. Coupling of XRDT and DSC data demonstrates that at least a less stable → more stable transition is observed during heating at 1 °C/min following AGMF cooling at 1 °C/min.

2. Crystallization Behavior of AGMF at 5 °C/min. *2.1. Cooling at 5 °C/min.* 2.1.1. Structural Analysis. The crystallization behavior of the AGMF was monitored, at fast cooling rate (5 °C/min) from 45 to −20 °C, by using the coupled XRDT/DSC technique, in order to complement the study of the formation of unstable crystalline forms of TGs. The SAXD and WAXD patterns recorded as a function of temperature are presented as 3D views in **Figure 6A**,**B**, respectively. At small angles (**Figure 6A**) and for $T \leq 12$ °C, five XRD peaks are recorded at about $q = 0.09$ (71.5 Å), 0.13 (46.7 Å), 0.16 (38 Å), 0.17 (36.4 Å), and about 0.26 Å^{-1} (24 Å). These lines correspond to the quasi-simultaneous crystallization at $T \leq$ 12 °C of two species, α3L (71.5 Å) and α$2L_1$ (46.7 Å), followed by that of a third species, $2L_2$ (38 Å). These species are similar to that observed during crystallization at 1 °C/min (**Figure 2**). At wide angles, the same α → sub α transition as above is observed.

2.1.2. Thermal Properties. The crystallization curve recorded simultaneously with XRDT experiments by DSC during the cooling of AGMF at 5 °C/min is presented in the insert of **Figure 6**. The curved shape of the DSC curve, at $T > 20$ °C, corresponds to the equilibration of the calorimeter. The DSC recording shows two overlapped exothermal events. The initial crystallization temperature occurs at about 12 °C. The first exotherm is related to crystallization of both α 3L (71.5 Å) and α $2L_1$ (46.7 Å) varieties. The second exotherm visible as a weak change of the peak decreasing slope at about −4 °C corresponds to a combination of the crystallization of the third species $2L_2$ (38 Å), likely superimposed with the transition α → sub α.

2.2. Subsequent Heating at 1 °C/min. Following cooling at 5 °C/min, the AGMF sample was immediately heated from −20 to 45 °C at 1 °C/min as previously.

2.2.1. Structural Analysis. XRDT patterns recorded simultaneously at small and wide angles during heating of AGMF are plotted as 3D views in **Figure 7A**,**B**, respectively. On heating at 1 °C/min, following fast cooling at 5 °C/min, the thermal evolution of the small angle patterns is similar to that observed above after slower cooling (1 °C/min). However, the lines of unstable forms at 46 and 38 Å are more marked while the intensity of lines of the main species is relatively less important (**Figure 8**). As a result, the IGOR analysis of peak position and intensity is able to separate the two lines at 38.1 and 36.4 Å all along the heating while this was not possible previously (**Figure 5**). On heating, the following polymorphic transitions are observed at wide angles: sub α ↔ α → β → liquid. They correspond to transitions and LS changes:

$$3L + 2L_2 + 2L_1 \rightarrow 2L_3$$

$$71\ \text{Å}\ \ 46\ \text{Å}\ \ 38\ \text{Å} \rightarrow 40\ \text{Å}$$

delimiting the various crystalline domains of existence.

While a monotropic polymorphic evolution α → β (in addition to the enantiotropic transition sub α ↔ α) was clearly observed independently at both small and wide angles but

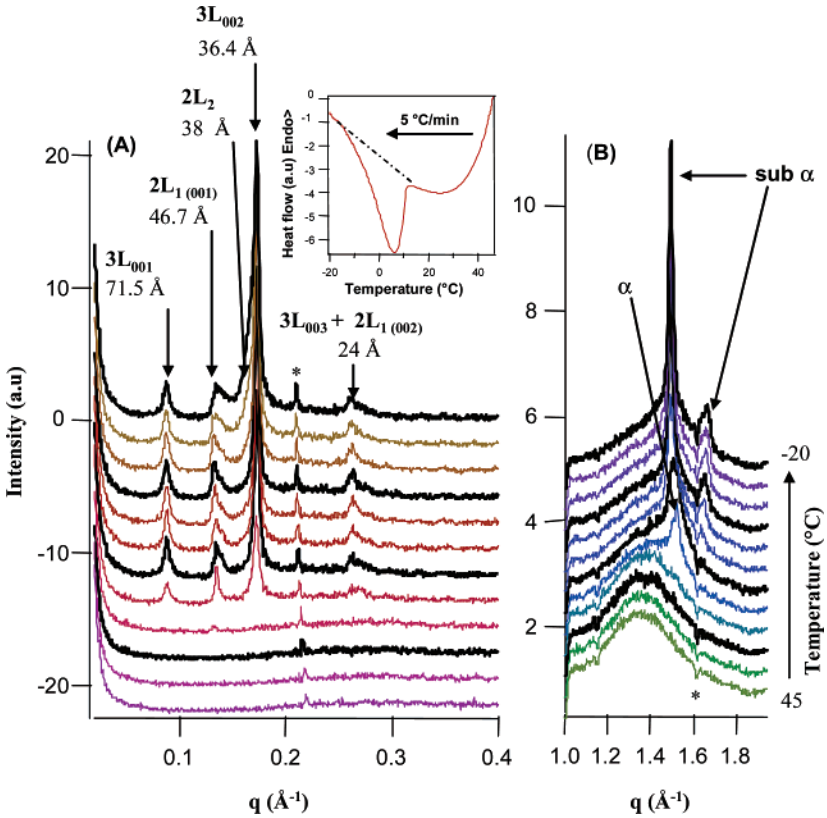

Figure 6. Three-dimensional plots of SAXD (**A**) and WAXD (**B**) patterns recorded as a function of time of AGMF at fast cooling rate 5 °C/min, using coupled XRDT-DSC. (The asterisk symbol corresponds to a negative peak due to the wide-angle detector defects.) The crystalline structures identified are noted on the figure. The insert shows the DSC crystallization curve recorded simultaneously during cooling of AGMF at 5 °C/min.

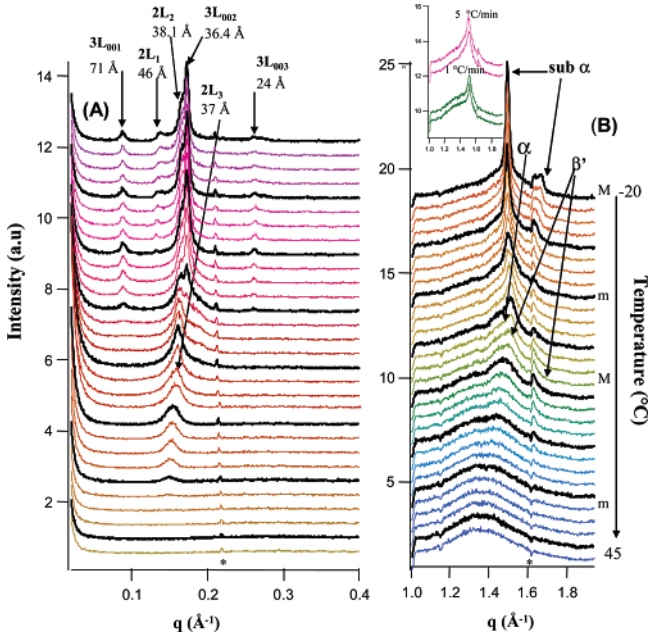

Figure 7. Three-dimensional plots of SAXD (**A**) and WAXD (**B**) patterns recorded as a function of time during heating of AGMF at 1 °C/min after cooling at 5 °C/min (asterisk as above **Figure 2**). The crystalline structures identified are noted in the figure. The insert shows a comparison of the lines shapes observed at wide angles upon heating at 1 °C/min, after cooling at 5 and 1 °C/min.

concomitantly, it was not possible to determine further exactly which species disappeared to the benefit of which. However, taking into account the final melting point of this phase, the TGs involved in this transition are likely the long chain trisaturated or the monounsaturated ones as evidenced for ABMF. It is worth noting that the line shapes observed at wide angles upon heating at 1 °C/min, after cooling at 5 and 1 °C/min, are significantly different as shown in the insert of **Figure 7B**. The lines observed after cooling at 5 °C/min are broader than those recorded after cooling at 1 °C/min.

2.2.2. Thermal Analysis. The DSC curve recorded simultaneously with XRDT experiments is presented in **Figure 8**. On the melting curve recorded, the different ranges observed can be tentatively analyzed as following. The first endotherm, low melting point fraction (LMPF), corresponds to melting of $\alpha 2L_1$ and $\alpha 3L$ structures. The second endotherm, middle melting point fraction (MMPF), corresponds to that of $\beta' 2L_2$. The last endotherm, high melting point fraction (HMPF), coincides with the melting of $\beta' 2L_3$ until final melting.

Concerning the reversibility of the sub $\alpha \leftrightarrow \alpha$ transition, which precedes the $\alpha \rightarrow \beta'$ one, the $\alpha \rightarrow$ sub α transition is clearly evidenced on cooling on both WAXD pattern evolutions of **Figures 2B** and **6B**. On heating, the reversibility of this transition is attested by the sub $\alpha \leftrightarrow \alpha$ changes observed in **Figures 4B** and **7B** [the variations of intensity of the line at 3.8 Å are illustrated by small (m) and capital (M) letters indicative of minimum and maximum, respectively, in **Figure 7**]. However, we cannot rule out the possible transition of part of the sub α liquid crystals directly to the crystalline form β'. The first minimum of this line, which is less marked after slower cooling (**Figure 4**) than in **Figure 7**, seems to indicate at least a partial direct sub $\alpha \rightarrow \beta'$ transition.

3. Crystallization Behavior of AGMF after Quenching. *3.1. Isothermal Conditioning at −20 °C after Quenching.* A sample of melted AGMF was fast crystallized by quenching

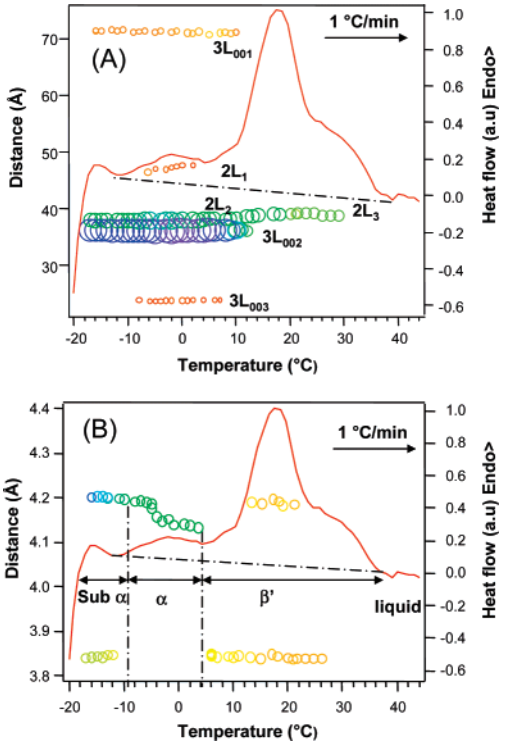

Figure 8. Evolutions, as a function of temperature of the LS (**A**) and SS (**B**) deduced from the diffractions peaks of **Figure 7** as above, are superimposed with the DSC crystallization curve recorded simultaneously during heating of AGMF at 1 °C/min following its crystallization cooling at 5 °C/min. Symbol sizes, centered on distance and temperature, are proportional to the maxima intensities of the diffraction peaks.

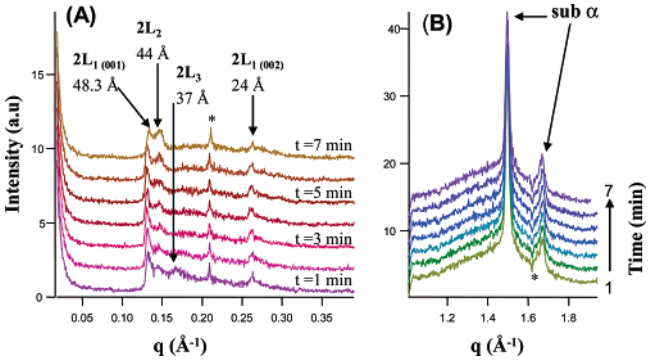

Figure 9. Three-dimensional plots as a function of time of SAXD (**A**) and WAXD (**B**) patterns recorded from AGMF after quenching to −20 °C (asterisk as above **Figure 2**). The crystalline structures identified are noted in the figure.

from 45 to −20 °C with the procedure applied to the study of ABMF and cocoa butter polymorphism (*15*, *26*). We introduced directly the capillary, containing the melted sample at 45 °C, into the calorimeter maintained at −20 °C in isothermal conditions. The quenching temperature was chosen low enough to rapidly freeze the sample in the less stable polymorphic varieties. Then, the evolution of these less stable forms toward more stable varieties was analyzed during the heating of the sample at 1 °C/min as previously described.

The SAXD pattern (**Figure 9A**) immediately recorded at −20 °C shows four peaks observed at q = 0.13, 0.14, 0.17, and 0.26 Å^{-1} corresponding to LS = 48.3, 44, 37, and 24 Å. All of the peaks observed correspond to the formation of bilayered structure (2L). The sharp line at 24 Å may be attributed to the second-order $2L_{1(002)}$ of the sharp line observed at

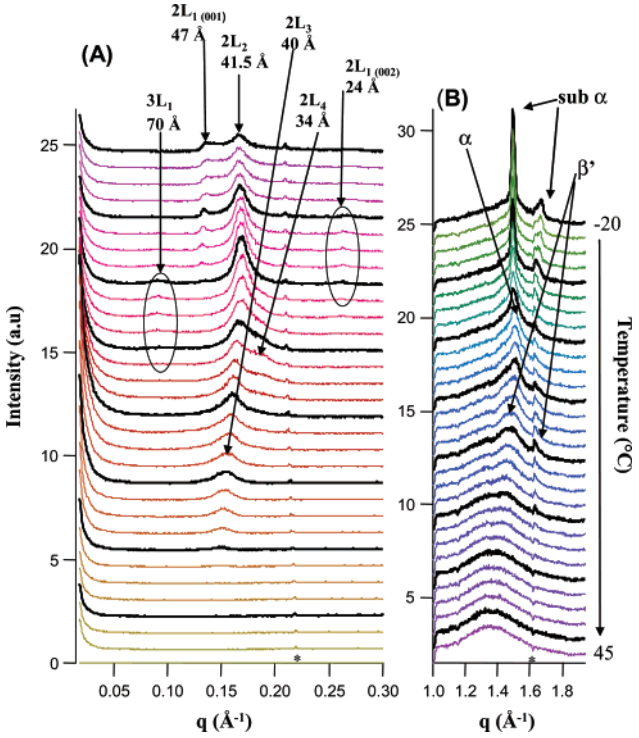

Figure 10. Three-dimensional plots of SAXD (**A**) and WAXD (**B**) patterns recorded as a function of time during the heating of AGMF at 1 °C/min following its quenching (asterisk as above **Figure 2**). The crystalline structures identified are noted in the figure.

$2L_{1(001)}$ = 48.3 Å. As a function of time, the intensity of this $2L_{1(001)}$ line slightly decreased while that of its neighbor at LS = 44 Å increased. The intensity of the broad line named $2L_3$ vanished within 2 min. Such fast evolution of SAXD lines was already observed for ABMF but with different species (LS = 71 and 47 Å against LS = 48, 44, and 37 Å in this study). The WAXD pattern (**Figure 9B**) evidenced two diffraction lines at q = 1.49 (4.2 Å) and 1.66 Å^{-1} (3.7 Å), which are characteristic of TGs crystallization with an orthorhombic perpendicular packing of the acylglycerols chains (sub α), which was not observed for ABMF.

3.2. Heating of Quenched AGMF at 1 °C/min from −20 to 45 °C. 3.2.1. Structural Analysis. After conditioning at −20 °C, the sample of AGMF examined above has been heated in the calorimeter to 45 °C with a heating rate of 1 °C/min as previously described. The SAXD patterns recorded as a function of time are plotted in **Figure 10A** vs temperature as 3D viewing. These XRD patterns show successively, as a function of temperature, the vanishing of the diffraction lines of the 2L species initially formed and their replacement by more stable 2L and 3L forms. Six domains can be temperature-delimited corresponding to the successive transitions:

$$2L_1 + 2L_2 \rightarrow 3L_1 + 2L_2 \rightarrow 3L_1 + 2L_2 + 2L_3 \rightarrow 2L_2 + 2L_3 \rightarrow 2L_4 \rightarrow \text{liquid}$$

At wide angles, the succession of transitions is

$$\text{sub } \alpha \leftrightarrow \alpha \rightarrow \beta' \rightarrow \text{liquid}$$

Because they all transformed into more stable forms, we concluded, as already observed for many fats including ABMF, that all forms obtained by quenching are highly metastable even compared to that observed above at intermediate cooling rates (*18*, *20*, *26*, *28*).

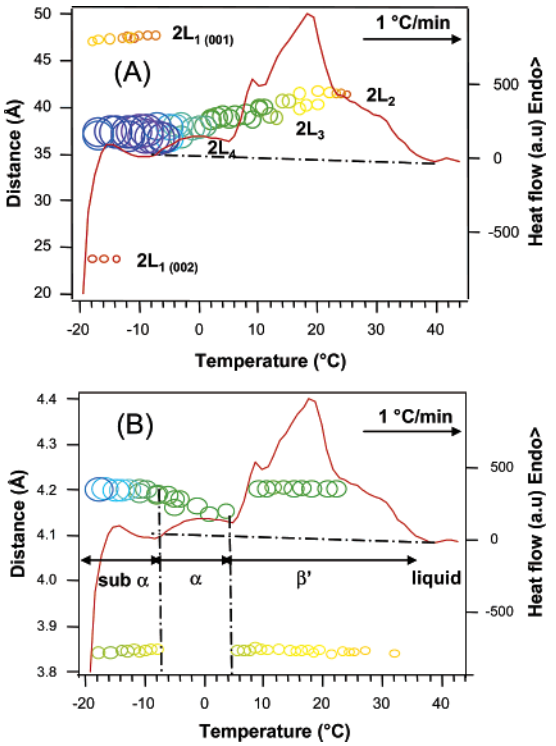

Figure 11. Evolutions, as a function of temperature of the LS (**A**) and SS (**B**) deduced from the diffractions peaks of **Figure 10** as above, are superimposed with the DSC crystallization curve recorded simultaneously during heating of AGMF at 1 °C/min following its quenching. Symbol sizes, centered on distance and temperature, are proportional to the maxima intensities of the diffraction peaks.

3.2.2. Thermal Analysis. The DSC melting curve (**Figure 11**) was recorded, simultaneously with XRD as a function of temperature, during heating at 1 °C/min from the same sample of AGMF quenched at −20 °C, thanks to XRDT/DSC coupling. While numerous transitions are observed by XRD, surprisingly, the DSC recording apparently shows the only four melting endotherms observed above after cooling at 1 °C/min (**Figure 5**). Then, apparently, DSC would not be sensitive to the melting/reorganization of the less stable crystalline varieties. Their enthalpies are possibly small as compared to melting enthalpies of crystals of intermediate stability. However, more detailed observation and comparison with the heating recording was observed after cooling at 5 °C/min. **Figure 8** shows that an additional sharp endotherm is observed in the range 8−10 °C. While the attribution of all others endotherms are straightforward, thanks to XRDT recording analysis (being similar to that discussed above, it will not be detailed here), that of the supplementary peak is tentatively attributed to the rapid crystallization and melting of the 3L structure (only briefly observed on **Figure 10A**).

4. Influence of the Cooling Rate on the Thermal and Structural properties of AGMF. *4.1. Thermal Behavior.* The thermal behavior of AGMF was monitored by DSC on cooling at different rates ranging from 0.1 to 5 °C/min (**Figure 12A**) and then immediately on heating at the same rate, 1 °C/min, in order to study both the direct influence of the cooling rate and the evolution of crystalline structures during their melting (**Figure 12B**). The recording observed on heating after sample quenching has been added for comparison.

Both sets of recordings show that the initial temperature of crystallization measured and the shape of the crystallization and melting curves depend on the cooling rate used. On the one hand, **Figure 12A** shows that the initial temperature of crystallization of AGMF decreases with the increasing of cooling rate. The temperature shift is related to the rate through the process of crystal nucleation (*24*). On the other hand, our results show the existence of four to three exotherms at slow and intermediate cooling rates (0.1 and 1 °C/min), whereas only two exotherms have been observed on fast cooling of the AGMF at 5 °C/min. Our results are similar to others of ABMF (*18*) but are more complex to interpret since less exotherms are observed during crystallization of AGMF than for ABMF. While identification of the crystallization of the different species was rather easily done using coupling of DSC and XRDT recordings for ABMF (*15*−*18*), that of AGMF was more delicate due to the superimposition of the thermal events. The exotherms at 0.1 and 5 °C/min are hardly detected as a consequence; we need a more precise resolution and experimental conditions. There are two types of exotherms, a sharp peak corresponding to the crystallization of 2L forms and a broad one related to 3L packing. The number of thermal events overlapping each other increases

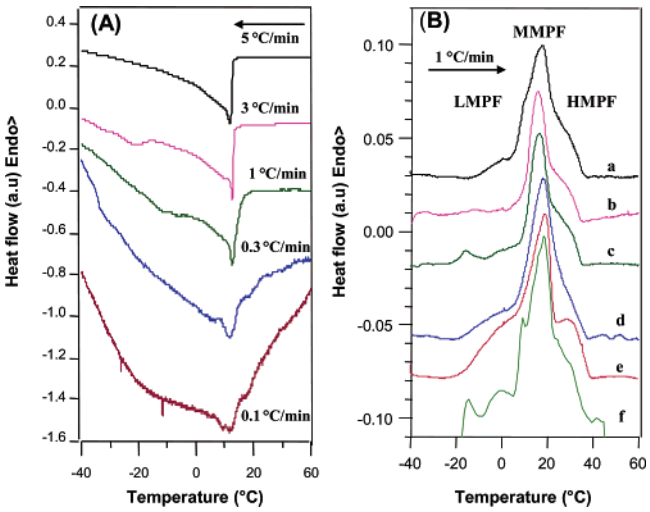

Figure 12. Influence of cooling rate on AGMF DSC recordings. (**A**) Crystallization curves recorded during cooling of AGMF from 60 to −40 °C/min at different cooling rates as indicated on the figure. (**B**) Corresponding melting curves recorded on heating at 1 °C/min, immediately after cooling at 5 (a), 3 (b), 1 (c), 0.3 (d), and 0.1 °C/min (e) and after quenching (f) (this DSC melting curve is recorded using coupled XRDT-DSC, not DSC-7).

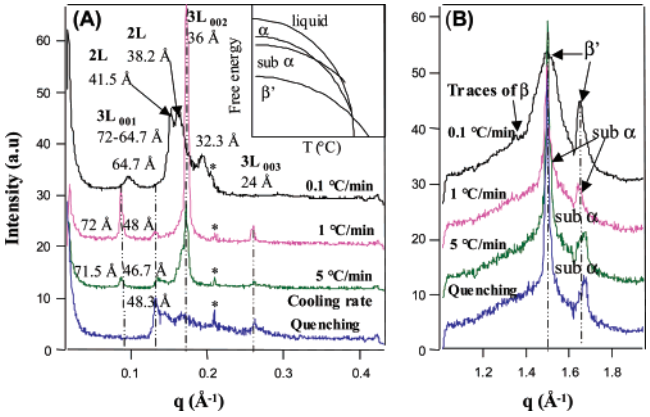

Figure 13. XRD patterns recorded at −20 °C at (**A**) small and (**B**) wide angles after either cooling of AGMF at the different cooling rates indicated on the figure or quenching at −20 °C. Insert: illustration by a free energy diagram of the types of transition encountered as a function of temperature, time, etc.

Table 1. Summary of the Structural and Thermal Characteristics Observed for AGMF by XRDT and DSC after Cooling at Different Rates Indicated and during Melting at 1 °C/min

cooling rate	0.1 °C/min	1 °C/min	5 °C/min	quenching
		thermal events		
no. of crystallization exotherms	3 (or 4 + 1 exotherm)	2	2	
initial temperature of crystallization (°C)	26	18	12	
final melting temperature (°C)	40	37	37	38
		varieties observed on cooling		
chain packing	α then β′ β (trace)	α ↔ sub α	α ↔ sub α	sub α
molecule stacking	$2L_1$ (41.5 Å)	3L (72.4, 36.4, 24.2, 18 Å)	$3L_{001}$ (71.5, 36.4, 24 Å)	$2L_1$ (48.3, 24 Å)
	$3L_1$ (72, 35.3 Å) $3L_2$ (64.7, 32.3 Å) $2L_2$ (38.2 Å)	2L (48 Å)	$2L_1$ (46.7, 24 Å) $2L_2$ (38 Å)	$2L_2$ (44 Å) $2L_3$ (37 Å)
		thermal behavior on heating at 1 °C/min		
chain packing	β′ and traces of β	sub α ↔ α or α → β′	sub α ↔ α → β′	sub α ↔ α → β′
longitudinal transition	no polymorphic transition	polymorphic transitions	polymorphic transitions	polymorphic transitions
DSC melting events	four endotherms (LMF, MMF, one or two HMF)	four endotherms (LMF, MMF, and HMF) and one exotherm	four endotherms (LMF, MMF, and HMF) and one exotherm	five endotherms (LMF, MMF, and HMF) and two exotherms

with the decrease of cooling rate because of the complex polymorphism of this TGs mixture. Indeed, slow cooling of AGMF favors the formation of stable species whereas fast cooling induces the crystallization under unstable varieties.

The "absence of transition on heating" criterion has been used to assess the relative stability of the crystalline phases formed on cooling (*11*, *12*, *18*). A standard heating rate of 1 °C/min, after the samples were cooled at different cooling rates from quenching to 0.1 °C/min, has been chosen to allow relatively slow transitions to occur while keeping DSC sensitivity at a high signal/noise ratio. The set of DSC curves recorded in these conditions is shown in **Figure 12B**. The overlapping of several endotherms is observed until the final melting temperature at about 38 °C. For intermediate cooling rates, they correspond to three different temperature ranges, respectively: $-18 < T < 6$ °C, $6 < T < 24$ °C, and $24 < T < 37$ °C. These temperature ranges observed do not correspond to that of ABMF (*18*). It is interesting to note that at (i) intermediate and faster cooling rate, the endotherms are less separated and (ii) the number of apparent endotherms increases with the cooling rate up to six for quenched sample. However, the final melting temperatures observed from the different cooling rates are not significantly different (**Figure 12B**). As a consequence, the final melting point of AGMF is apparently quite independent of the cooling rate.

Researchers agree on the existence on heating of ABMF of three overlapping endotherms corresponding to separate groups of TGs that melt separately (*28*, *29*). Although AGMF shows significant differences with ABMF, this classification of endotherms with low, medium, and high melting point fractions noted, respectively, LMPF, MMPF, and HMPF, can be applied here at least for melting corresponding to the intermediate cooling rate from 0.3 to 3 °C/min. The first endotherm corresponds to melting of 3L structures. The second and the third correspond to the melting of the 2L structures formed during cooling. The identification of the thermal events of more complex recordings in which transitions endotherms and exotherms superimpose to the above recordings (e.g., that observed after quenching) require complementary structural analysis.

4.2. Structural Behavior. The SAXD and WAXD patterns recorded at −20 °C after completion of cooling's AGMF, at different rates 0.1, 1, and 5 °C/min, and after quenching are presented in (**Figure 13A**,**B**). All SAXD patterns are different while only WAXD patterns recorded at 0.1 °C/min are really different of those observed after cooling at other rates. This clearly shows (i) that the thermal behavior applied directly influences the crystalline structures formed by TGs in AGMF, (ii) full characterization of these crystalline structures is only obtained at small angle, and (iii) both the synchrotron X-ray radiation and the long distance bench (here about 1.8 m) are requested to distinguish all species and their evolutions. **Table 1** summarizes the main structural characteristics of the species formed as well as that of their thermal transitions. The lamellar structures formed by TGs molecules on cooling at intermediate (1 °C/min) and fast cooling (5 °C/min) are close. They correspond to the coexistence of a main phase $3L_1$ (71.5−72 Å) and a 2L (47−48 Å); both apparently, depending on temperature, show either a hexagonal subcell noted α or a sub α. Both species are different from those observed after quenching or after slow cooling. While quenching leads to similar sharp, WAXD patterns of sub α type, the SAXD shows highly disorganized 2L molecular stackings characterized by a main line at 48 Å and other broader lines. The reverse situation is observed for the patterns recorded after slow cooling (0.1 °C/min). The SAXD pattern is characterized by rather broad lines at 64.7, 41.5, and 38.2 Å corresponding to 3L and 2L stackings while the chain packing is mainly of β′ type with traces of β, which are absent on cooling at 1 and 5 °C/min.

Comparison of widths of the lines reported in **Figure 13** clearly evidences the differences between the crystalline species obtained at slow cooling and the liquid-crystalline phases obtained at faster rates. Sharp lines observed at intermediate cooling rates correspond to the tight sub α lateral packing of chain associated with a loose longitudinal organization of mainly vertical chains, the former being rendered possible by the latter, which give to the chains the necessary degrees of freedom. On the contrary, in the crystalline packings of the slowly cooled species, both chains and molecules are ordered. The chains are tilted, tightly laterally packed in orthorhombic perpendicular subcell and methyl terminal ends of chains pilled the most tightly possible as shown by the presence of traces of β form. In the

crystalline form, free energy is minimized by packing molecules longitudinally the best possible. As a result, there is broadening of the lines corresponding to lateral packing as clearly shown **Figure 13**.

The reversible α ↔ sub α transition is only observed at a cooling rate ≥1 °C/min. However, at an intermediate cooling rate of 1 °C/min, some irreversible transition α → β′ has already occurred as shown by the comparison of WAXD line widths at 1 and 5 °C/min. Nevertheless, the process of organizing a large variety of TGs in β′ form is very slow; it might take hours, if not days, to fully organize crystals (*18*). This demonstrates that full characterization of the thermal and structural behaviors of a fat requires precise observations at both wide and small angles together with DSC at a broad range of rates, as already observed for lard and ABMF (*11*, *18*). The cooling rate plays an important role in crystallization behavior and it frequently determines the size and the nature of crystals at macroscopic scale (*27*). Indeed, at the molecular scale, the variation of cooling rate is one of the major tools allowing exploration of the thermal and structural behaviors of fats.

To the author's knowledge, this is the first dynamic study performed as a function of time and temperature, to characterize the crystallization properties of GMF, at a molecular level. The use of the synchrotron radiation allowed us to study the polymorphism and phase transitions displayed by complex TGs mixtures, as a function of temperature, and to compare these data with DSC recording. These tools revealed the existence of two different forms 3L (α and β′) and numerous 2L (α and β′) in AGMF depending on crystallization conditions. Although the dominant stable form is β′, four different polymorphic subcell types, sub α, α, β′, and β, were observed. Monotropic (irreversible) transitions 3Lα → 3Lβ′ and 2Lα → 2Lβ′ were clearly identified, suggesting that some classes of mixed crystals may possibly undergo phase transitions at constant composition. Finally, it has been shown that the reversibility of the sub α ↔ α phase transition depends on the rate of temperature scan. Interestingly, this demonstrates that even in complex mixtures of triglycerides, reversible transition between metastable states exits. However, in our opinion, the fact that some reversibility of a transition exists does not allow us to call it "enantiotropic" since this term should be only employed for systems at equilibrium, which is not the case here (see insert in **Figure 13A**). It is also interesting to remark from this study the absolute need for high resolution at small angles and for temperature scans with coupled techniques. This is clearly illustrated in **Figures 12** and **13**. DSC recordings are quite similar, whatever the scanning rate, and WAXD only allows partial identification of molecular packings. Then, from this observation, we would like to stress the point that even a combination of DSC and XRD studies of fats would not warrant against misinterpretation of the polymorphic behavior, if they are not associated with systematic scans, at a broad set of cooling rates and high-resolution SAXD from the same sample (*11*, *12*, *18*).

We also concluded that although some general similitude exists in the thermal and structural properties of bovine and goat milk fat, they also evidence significant specific differences in the expression of their polymorphism, which are in relation with the diversity of TGs and FA compositions. Regarding the results obtained in this paper, such information increases the knowledge of the structure's complex fat in dairy products, which is of tremendous importance to better understand, control, and improve the physical properties (rheological, technological, functional, nutritional, and sensory) of AGMF's products.

ABBREVIATIONS USED

AGMF, anhydrous goat's milk fat; GMF, goat's milk fat; ABMF, anhydrous bovine's milk fat; TGs, triacylglycerols; DSC, differential scanning calorimetry; FA, fatty acids; 3L, trilayered stacking; 2L, bilayered stacking; SAXD, small-angle X-ray diffraction; WAXD, wide-angle X-ray diffraction; XRDT, X-ray diffraction as a function of temperature; XRD, X-ray diffraction; LS, long spacing; SS, short spacing; LMPF, low melting point fraction; MMPF, middle melting point fraction; HMPF, high melting point fraction.

ACKNOWLEDGMENT

We gratefully acknowledge Dr. Christelle Lopez for useful discussions and pertinent advice. We thank Dr. Jean Blaise Brubach for his assistance on the use of the IGOR software. We acknowledge Dr. T. Khorchani (Arid Region Institute, Medenine, Tunisia) for providing goat's milk.

LITERATURE CITED

(1) Billon, P. Milking management. In *Encyclopedia of Dairy Sciences*; Roginski, H., Fuquay, J. W., Fox, P. F., Eds.; Academic Press: Cornwall, 2003; pp 1243−125.

(2) Zan, M.; Stibilj, V.; Rogelj, I. Milk fatty acid composition of goats grazing on alpine pasture. *Small Ruminant Res*. **2006**, *64*, 45−42.

(3) Isachi, S. P. A.; Hui, J.; Chong, F. N.; Strange, A.; Bencini, R.; Tay, G. K. Comparison of the milk quality of the South African Boer and Australian Rangeland goats. *Small Ruminant Res*. **2004**, *53*, 181−184.

(4) Haenlein, G. F. W. Goat milk in human nutrition. *Small Ruminant Res*. **2004**, *51*, 155−163.

(5) Christie, W. W. Composition and structure of milk lipids. In *Advanced Dairy Chemistry*, 2nd ed.; Fox, P. F., Ed.; Chapman & Hall: London, United Kingdom, 1995; Vol. 2, pp 1−28.

(6) Jensen, R. G.; Ferris, A. M.; Lammi−Keefe, C. J. The composition of milk fat. *J. Dairy Sci*. **1999**, *74*, 3228−3243.

(7) Gresti, J.; Bugaut, M.; Maniongui, C.; Bezard, J. Composition of molecular species of triacylglycerols in bovine milk fat. *J. Dairy Sci*. **1993**, *76*, 1850−1869.

(8) Walstra, P.; van Beresteyn, E. C. H. Crystallization of milk fat in the emulsified state. *Neth. Milk Dairy J*. **1975**, *29*, 35−65.

(9) Small, D. M. The physical chemistry of lipids. From alkanes to phospholipids. In *Handbook of Lipid Research*; Hanahan, D. J., Ed.; Plenum Press: New York, 1986; pp 347−382.

(10) Keller, G.; Lavigne, F.; Loisel, C.; Ollivon, M.; Bourgaux, C.; Lesieur, P. Investigation of the complex thermal behavior of fats. *J. Therm. Anal*. **1996**, *47*, 1545−1565.

(11) Kalnin, D.; Lesieur, P.; Artzner, F.; Keller, G.; Ollivon, M. Systematic investigation of lard polymorphism using combined DSC and time-resolved synchrotron X-ray diffraction. *Eur. J. Lipid Sci. Technol*. **2005**, *107*, 594−505.

(12) Sato, K. Polymorphism of pure triacylglycerols and natural fats. *In Advances in Applied Lipid Research*; JAI Press Inc.: Amsterdam, The Netherlands, 1996; Vol. 2, pp 213−268.

(13) Kalnin, D.; Schafer, O.; Amenitsch, H.; Ollivon, M. Fat crystallization in emulsion: Influence of emulsifier concentration on triacylglycerol crystal growth and polymorphism. *Cryst. Growth Des*. **2004**, *4*, 1283−1293.

(14) Lavigne, F. *Polymorphisme et Transitions de Phases des Triglycérides. Applications aux Propriétés Thermiques et Structurales de la Matière Grasse Laitière Anhydre et de ses Fractions*; Univ. Paris VII: Paris XI et ENSIA, 1995.

(15) Lopez, C.; Lesieur, P.; Bourgaux, C.; Ollivon, M. Thermal and structural behavior of milk fat. 1. Unstable species of anhydrous milk fat. *J. Dairy Sci*. **2001**, *84*, 756−766.

(16) Lopez, C.; Lesieur, P.; Keller, G.; Ollivon, M. Thermal and structural behavior of anhydrous milk fat. 2. Crystalline forms obtained by slow cooling. *J. Dairy Sci*. **2001**, *84*, 2402−2412.

(17) Lopez, C.; Lesieur, P.; Ollivon, M. Crystalline structures formed in cream and anhydrous milk fat at 4 °C. *Lait* **2002**, *82*, 317−335.
(18) Lopez, C.; Lesieur, P.; Ollivon, M. Thermal and structural behavior of anhydrous milk fat: 3. Influence of cooling rate. *J. Dairy Sci*. **2005**, *88*, 511−526.
(19) Karray, N.; Lopez, C.; Lesieur, P.; Ollivon, M. Dromedary milk fat: Thermal and structural properties 1—Crystalline forms obtained by slow cooling. *Lait* **2004**, *84*, 399−416.
(20) Karray, N.; Lopez, C.; Lesieur, P.; Ollivon, M. Dromedary milk fat: Thermal and structural properties 2—Influence of cooling rate. *Lait* **2005**, *85*, 433−451.
(21) Ben Amara-Dali, W.; Karray, N.; Lesieur, P.; Ollivon, M. Anhydrous goat's milk fat: Thermal and structural behavior. 1. Crystalline forms obtained by slow cooling. *J. Agric. Food Chem.* **2005**, *53*, 10018−10025.
(22) Keller, G.; Forte, L.; Andrieux, K.; Dahim, M.; Loisel, C.; Ollivon, M.; Bourgaux, C.; Lesieur, P. DSC and X-ray diffraction coupling. Specifications and applications. *J. Therm. Anal.* **1998**, *51*, 783−791.
(23) Ollivon, M.; Keller, G.; Bourgaux, C.; Kalnin, D.; Villeneuve, P.; Lesieur, P. DSC and high resolution X-ray diffraction coupling. *J. Therm. Anal. Calorim.* **2006**, *85*, 219−224.
(24) Lopez, C.; Bourgaux, C.; Lesieur, P.; Bernadou, S.; Keller, G.; Ollivon, M. Thermal and structural behavior of milk fat: 3. Influence of cooling rate and droplet size on cream crystallization. *J. Colloid Interface Sci.* **2002**, *254*, 64−78.
(25) Lavigne, F.; Bourgaux, C.; Ollivon, M. Phase transition of saturated triglycerides. *Suppl. J. Phys. I* **1993**, *3*, 137−140.
(26) Loisel, C.; Keller, G.; Lecq, G.; Bourgaux, C.; Ollivon, M. Phase transition and polymorphism of cocoa butter. *J. Am. Oil. Chem. Soc*. **1998**, *75*, 425−439.
(27) Marangoni, A. G. *Fat Crystal Networks*; Food science and technology series; Marcel Dekker Inc.: New York, 2005; Vol. 140, pp 850.
(28) Timms, R. E. The phase behavior and polymorphism of milk fat, milk fat fractions, and fully hardness milk fat. *J. Dairy Technol*. **1980**, *35*, 47−53.
(29) Marangoni, A. G.; Lencki, R. W. Ternary phase behavior of milk fat fractions. *J. Agric. Food Chem.* **1998**, *46*, 3879−3884.

Received for review November 7, 2006. Revised manuscript received January 22, 2007. Accepted February 11, 2007.

JF063210P